



UNIVERSITY OF
ARKANSAS

The classical fifth order WENO based
Numerical Simulations of Richtmyer-Meshkov Instability

Tulin Kaman
tkaman@uark.edu

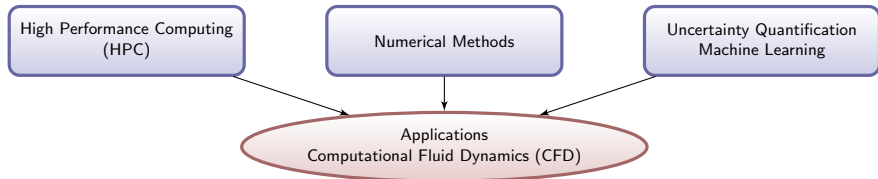
Department of Mathematical Sciences
Fulbright College of Arts and Science
Lawrence Jesser Toll Jr. Endowed Chair

University of Arkansas, Fayetteville

The Center for Computational & Applied Mathematics (CCAM) Workshop on
Numerical Methods for Hyperbolic Conservation Laws
May 9-10, 2022

Computational and Applied MATH group

<https://kaman.uark.edu>



- Validation & Verification : Numerical Simulations of Turbulent Mixing
- Quantify errors and uncertainties in multi-physics models and data



Simulations and Modeling of Turbulent Mixing

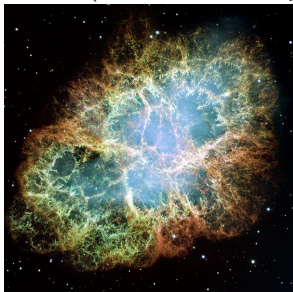
Rayleigh–Taylor Instability (RTI) :

arises at the interface between two fluids of different densities whenever the pressure gradient opposes the density gradient.

Richtmyer-Meshkov Instability (RMI) :

arises when a shock wave interacts with the interface. RMI is known as the impulsive or shock-induced RTI.

Photograph courtesy of NASA, ESA, J. Hester and A. Loll (Arizona State University)



Photograph courtesy of David Jewitt, University of California at Los Angeles.



Problem statement

- Growth rate of RTI, α_{RTI} ,

$$h = \alpha A g t^2$$

h , penetration distance of the light fluid into the heavy fluid

A , Atwood ratio = $(\rho_1 - \rho_2)/(\rho_1 + \rho_2)$

g , acceleration

- Growth rate of RMI, V_{RMI} ,

$$V_{RMI} = k h_0 A \Delta U$$

k , wave number

h_0 , initial perturbation

A , Atwood ratio = $(\rho_1 - \rho_2)/(\rho_1 + \rho_2)$

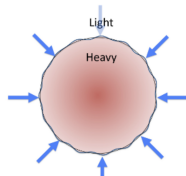
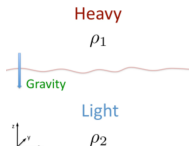
ΔU , interface velocity

Gravitational acceleration.

The heavy fluid is supported by the lighter fluid.

Inertial Confinement Fusion fuel capsule.

The lighter material is pushing on the heavier one



Numerical Approaches to Model Turbulent Flows

Three levels of numerical simulation for turbulent flows :

- Direct Numerical Simulation (DNS)
 - The full NSE is solved without any model for turbulence
 - The most demanding method among the three, very accurate
- Large Eddy Simulation (LES)
 - Flow field is resolved down to a certain length scale, and scales smaller than that are modeled rather than resolved
 - Computational cost higher than RANS, but much lower than DNS
- Reynolds Averaged Navier Stokes (RANS)
 - Time-averaged equations solving for the mean values of all quantities
 - The least demanding in terms of resources

The essential features of the algorithms are

- Large Eddy Simulations (LES) with subgrid scale (SGS) terms to model the diffusive transport corrections to the mesh (Reynolds) averaged Navier-Stokes equations. Coefficients in SGS models are determined from the simulation itself and the models are parameter free.

They are quite complex at a detailed level, have a very simple conceptual derivation. For example the Reynolds stress tensor, which for a nonlinear flux term F is the difference

$$F(\langle U \rangle) - \langle F(U) \rangle$$

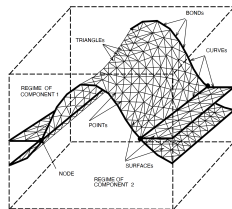
This difference is approximated by a term proportional to a gradient, ∇U . The problem is to determine the coefficient of proportionality. The missing coefficient is selected dynamically from the simulation.

- Front Tracking (FT), to achieve resolution of steep and sharp density gradients

Front Tracking (FT) I

Glimm, Grove, Li and Zhou 1998, 2000

- An adaptive computational method that provides sharp resolution of a wave front by tracking the interfaces between distinct materials.
- It represents interfaces explicitly as lower dimensional meshes moving through a rectangular grid. In 2D, the wave is represented by a curve which is comprised of connected line segments. In 3D, the wave is represented by a triangular mesh.
- The states (density, pressure and velocity) of fluids are located in the centers of each grid cell.
- The method solves the equations with the following main steps :
 - ① interface propagation
 - ② interpolation reconstruction,
 - ③ interior states update



Front Tracking API

These features are included in the multipurpose simulation code **FronTier**.

Performance of *FronTier*

- FronTier scales to the entire system on Argonne's IBM Blue Gene/P supercomputer - 163,840 cores
- Innovative and Novel Computational Impact on Theory and Experiment Awards
 - "Stochastic (w^*) Convergence for Turbulent Combustion"
 - "Uncertainty Quantification for Turbulent Mixing"

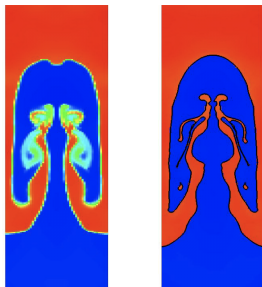


Figure – RTI single mode simulation at $t = 10s$. Comparison of a FLASH run without (left) and with (right) the use of front tracking API.

Model : Multiphase Navier-Stokes equations I

The mathematical formulation is based on the filtered Navier-Stokes equations for the multiphase flows :

- The variables filtered on the grid scale are denoted by the overbar.
- The density-weighted filtering operation is denoted by the tilde.

The Favre-filtered continuity equation is obtained by

- 1 applying the grid scale onto the continuity equation

$$\frac{\partial \bar{\rho}}{\partial t} + \frac{\partial \bar{\rho} v_i}{\partial x_i} = 0,$$

- 2 then the density-weighted filtering $\tilde{v}_i = \frac{\bar{\rho} v_i}{\bar{\rho}}$.

For the compressible flows, the Favre-filtered continuity equation

$$\frac{\partial \bar{\rho}}{\partial t} + \frac{\partial \bar{\rho} \tilde{v}_i}{\partial x_i} = 0$$

Model : Multiphase Navier-Stokes equations II

J. Glimm, D. H. Sharp, TK, H. Lim. New Directions for Rayleigh - Taylor Mixing. Phil. Trans. of the Royal Society A, 371, pp.183, 2013.

$$\begin{aligned} \frac{\partial \bar{\rho}}{\partial t} + \frac{\partial \bar{\rho} \tilde{v}_i}{\partial x_i} &= 0, \\ \frac{\partial \bar{\rho} \tilde{v}_j}{\partial t} + \frac{\partial (\bar{\rho} \tilde{v}_i \tilde{v}_j + \bar{p} \delta_{ij})}{\partial x_i} &= \frac{\partial \bar{d}_{ij}}{\partial x_i} - \frac{\partial \tau_{ij}}{\partial x_i}, \\ \frac{\partial \bar{E}}{\partial t} + \frac{\partial (\bar{E} + \bar{p}) \tilde{v}_i}{\partial x_i} &= \frac{\partial \bar{d}_{ij} \tilde{v}_j}{\partial x_i} + \frac{\partial}{\partial x_i} \left(\bar{\kappa} \frac{\partial \tilde{T}}{\partial x_i} \right) + \frac{\partial}{\partial x_i} \left((\tilde{H}_h - \tilde{H}_l) \bar{\rho} \tilde{D} \frac{\partial \tilde{\Psi}}{\partial x_i} \right) \\ &+ \left(\frac{1}{2} \frac{\partial \tau_{kk} \tilde{v}_i}{\partial x_i} - \frac{\partial q_i^{(H)}}{\partial x_i} - \frac{\partial q_i^{(T)}}{\partial x_i} - \frac{\partial q_i^{(V)}}{\partial x_i} \right), \\ \frac{\partial \bar{\rho} \tilde{\Psi}}{\partial t} + \frac{\partial \bar{\rho} \tilde{\Psi} \tilde{v}_i}{\partial x_i} &= \frac{\partial}{\partial x_i} \left(\bar{\rho} \tilde{D} \frac{\partial \tilde{\Psi}}{\partial x_i} \right) - \frac{\partial q_i^{(\Psi)}}{\partial x_i}. \end{aligned}$$

The dependent filtered variables $\bar{\rho}$, $\tilde{\Psi}$, \tilde{v}_i , \bar{p} , and \bar{E} the total mass, the species mass fraction, the velocity, the pressure and the total specific energy, with

$$\bar{E} = \bar{\rho} \tilde{e} + \bar{\rho} \tilde{v}_k^2 / 2 + \tau_{kk} / 2$$

Model : Multiphase Navier-Stokes equations III

\widetilde{H}_h and \widetilde{H}_l are the partial specific enthalpy of each species defined by

$$\widetilde{H}_h = \widetilde{e}_h + \frac{\overline{p}}{\overline{\rho}}, \quad \widetilde{H}_l = \widetilde{e}_l + \frac{\overline{p}}{\overline{\rho}},$$

where \widetilde{e}_h and \widetilde{e}_l are the specific internal energy of each species. The viscous stress tensor, d_{ij} , in momentum and energy equations is expressed as

$$\overline{d_{ij}} = \overline{v_d} \left(\left(\frac{\partial \widetilde{v}_i}{\partial x_j} + \frac{\partial \widetilde{v}_j}{\partial x_i} \right) - \frac{2}{3} \frac{\partial \widetilde{v}_k}{\partial x_k} \delta_{ij} \right),$$

where $\overline{v_d} = \overline{\rho v_k}$ is the filtered dynamic viscosity.

SGS variables :

$$\begin{aligned} \tau_{ij} &= \overline{\rho} (\widetilde{v}_i \widetilde{v}_j - \widetilde{v}_i \widetilde{v}_j) \\ q_i^{(H)} &= \overline{\rho} (\widetilde{c_p} \widetilde{T} v_i - \widetilde{c_p} \widetilde{T} \widetilde{v}_i) \\ q_i^{(T)} &= \frac{1}{2} \overline{\rho} (\widetilde{v}_k \widetilde{v}_k v_i - \widetilde{v}_k \widetilde{v}_k \widetilde{v}_i) \\ q_i^{(V)} &= \overline{d_{ij} v_j} - \overline{d_{ij}} \widetilde{v}_j \\ q_i^{(\Psi)} &= \overline{\rho} (\widetilde{\Psi} v_i - \widetilde{\Psi} \widetilde{v}_i) . \end{aligned}$$

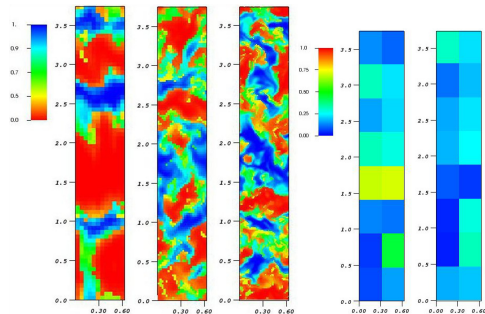
- Implemented in the code FRONTIER.
- Equation of state
- Time stepping 2nd order Runge-Kutta

Validation and Verification of Turbulent Mixing due to the multi-mode RTI

Kaufman, TK, Yu, Glimm. Stochastic Convergence and the Software Tool W*. Numerical Methods for Hyperbolic Equations, 2012

Turbulent Mixing due to Rayleigh-Taylor Instability within a rocket tank (Smeeton Youngs 1987)

- Heavy fluid concentration at the midplane, $t = 50$.
- For each supercell, we bin the concentration values into 5 bins, and count the number of values lying in each bin, to obtain a probability.
- We study integrated convergence through an L_1 norm (relative to integration both in solution state variables and over space-time) for the CDFs.
- Spatial array of L_1 norms of CDF mesh differences for heavy fluid concentrations at the midplane.



Validation and Verification of Turbulent Mixing due to the single mode RMI

TK, Holley, V&V of Turbulence Mixing due to Richtmyer-Meshkov Instability of an air/SF6 interface, IJNAM 22 (accepted). <https://kaman.uark.edu/research/publications/>
2D Euler equations of the compressible inviscid gases :

$$\mathbf{U}_t + \mathbf{F}(\mathbf{U})_x + \mathbf{G}(\mathbf{U})_y = 0$$

where \mathbf{U} , $\mathbf{F}(\mathbf{U})$ and $\mathbf{G}(\mathbf{U})$ are the vectors of conserved (mass, momentum, energy) variables and the fluxes in x and y direction.

$$\mathbf{U} = \begin{pmatrix} \rho \\ \rho u \\ \rho v \\ E \end{pmatrix}, \mathbf{F}(\mathbf{U}) = \begin{pmatrix} \rho u \\ \rho u^2 + p \\ \rho uv \\ (E + p)u \end{pmatrix}, \mathbf{G}(\mathbf{U}) = \begin{pmatrix} \rho v \\ \rho uv \\ \rho v^2 + p \\ (E + p)v \end{pmatrix}$$

Here ρ is the density, (u, v) is the velocity in (x, y) directions, p is the pressure, $E = \rho e + \frac{1}{2}\rho(u^2 + v^2)$ is the total energy $e = \frac{p}{(\gamma-1)\rho}$ is the specific internal energy γ is the constant specific heat ratio.

The Euler equations (1) are extended with the equation of concentration equation

$$\frac{\partial \rho M}{\partial t} + \frac{\partial \rho M u}{\partial x} + \frac{\partial \rho M v}{\partial y} = 0,$$

where M is the mass fraction for the heavy fluid.

Summary of the Weighted essentially non-oscillatory (WENO) Method

Jiang and Shu 1996, Balsara and Shu 2000, Shu 2020, Schilling and Latini 2004

flux-averaged WENO method uses local Lax-Friedrichs flux-splitting and a characteristic decomposition of the variables and fluxes*

- 1 compute the average state $\bar{\varphi}^\alpha$ at $(i + 1/2, j, k)$;
- 2 evaluate the left and right eigenvector matrices $L(\bar{\varphi})$ and $R(\bar{\varphi})$, and the eigenvalues of the Jacobian matrix at the average state;
- 3 for every stencil, project the conservative fields and the fluxes onto the local characteristic directions using the left eigenvector matrix ($2r - 1$ is the formal order of accuracy), $\varphi_{m,j,k}^{\alpha(ch)} = L(\bar{\varphi})\varphi_{m,j,k}^\alpha$ and $F_{m,j,k}^{\alpha(ch)} = L(\bar{\varphi})F_{m,j,k}^\alpha$ with $m \in [i - r + 1, i + r]$;
- 4 evaluate the left and right characteristic fluxes $\hat{F}_{m,j,k}^{\alpha(ch)\pm}$ pointwise value $F_{m,j,k}^\alpha$ using local or global Lax-Friedrichs flux-splitting;
- 5 reconstruct the numerical characteristic flux functions $\hat{F}_{m,j,k}^{\alpha(ch)\pm}$ from the pointwise values $F_{m,j,k}^\alpha$ using the WENO method
- 6 compute the numerical flux function in physical space by projecting back using the right eigenvector matrix $F_{i+1/2,j,k}^\alpha = R(\bar{\varphi})(F_{i+1/2,j,k}^{\alpha,+} + F_{i+1/2,j,k}^{\alpha,-})$
- 7 obtain the fluxes in the y- and z-directions $(i, j + 1/2, k)$ and $(i, j, k + 1/2)$ accordingly, and;
- 8 advance the solution one timestep using the second-order Runge-Kutta scheme, and compute a new timestep based on the CFL condition.

Problem 1 : Sod Shock Tube Problem I

For the contact discontinuity tracking,
Sod's shock tube problem which is a Riemann problem with initial condition

$$(\rho, u, p) = \begin{cases} (1, 0, 1) & \text{if } -5 \leq x \leq 0 \\ (0.125, 0, 0.1) & \text{if } 0 \leq x \leq 5 \end{cases} \quad (1)$$

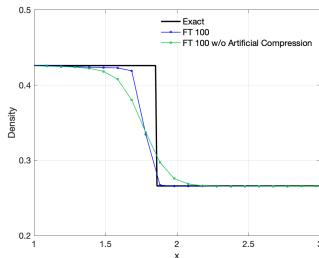
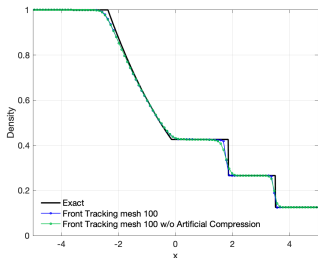
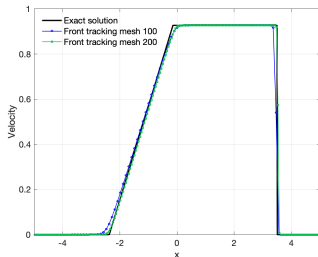
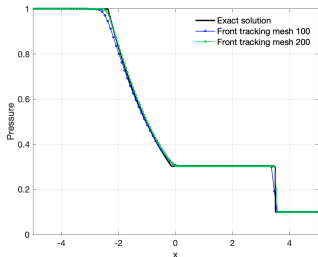


Figure – Left : The fifth order WENO scheme with and without artificial compression method of Yang are compared with the exact solution of Sod's shock tube problem. Right : A zoomed view on domain $[1, 3]$.

Problem 1 : Sod Shock Tube Problem II

Pressure and velocity profiles on 100 and 200 mesh points at $t=0.2s$ are compared with the exact solution of Sod's shock tube problem.

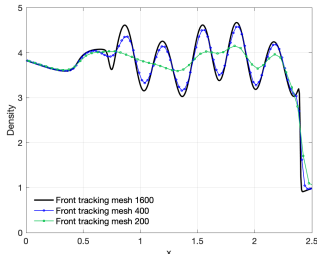
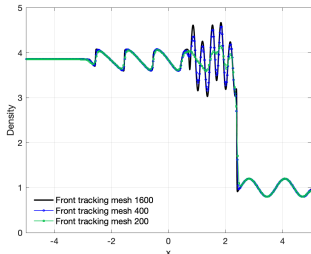


Problem 2 : Shock-entropy wave interaction (Shu-Osher) I

Study the stability and accuracy of the WENO scheme for strong shocks. Shu-Osher's test problem corresponds to a Mach $M = 3$ shock wave passing through an entropy wave on the spatial domain $(-5, 5)$ and the time domain $(0, 2)$.

$$(\rho, u, p) = \begin{cases} (3.857143, 2.629369, 10.33333) & \text{if } x \leq -4 \\ (1 + 0.2 \sin 5x, 0, 1) & \text{if } x \geq -4 \end{cases} \quad (2)$$

The solution near N-wave ($[-2, 0]$), the transition to the N-wave ($x \in [0, 1]$), the entropy wave ($x \in [1, 2]$), and the shock ($x \in [2, 2.5]$) is displayed under three levels of mesh refinement, 200, 400 and 1600 mesh points at $t = 1.8$.



Problem 3 : Richtmyer-Meshkov Instability I

For validation study, the model and input parameters are set according to the single mode RMI of Collins and Jacobs shock tube experiments for the two shock wave Mach numbers $M = 1.11$ and $M = 1.21$.

	Mach Numbers	
	1.11	1.21
Initial amplitude a_0 (cm)	0.229	0.183
Initial wavelength λ_0 (cm)	5.933	
Ratio between a_0/λ_0	0.0386	0.0308
Heavy fluid (SF ₆) density ρ_1 (g/cm ³)	5.944×10^{-3}	
Light fluid (air-acetone) density ρ_2 (g/cm ³)	1.351×10^{-3}	
Atwood number A	0.6053	
Molecular weight of SF ₆ (g/mol)	146.05	
Molecular weight of air-acetone (g/mol)	34.76	
Ratio of specific heats γ	1.276	
Pressure at interface p (bar)	0.956	
Courant–Friedrichs–Lewy (CFL) number	0.45	

Table – The parameter values of RMI simulations.

Problem 3 : Richtmyer-Meshkov Instability II

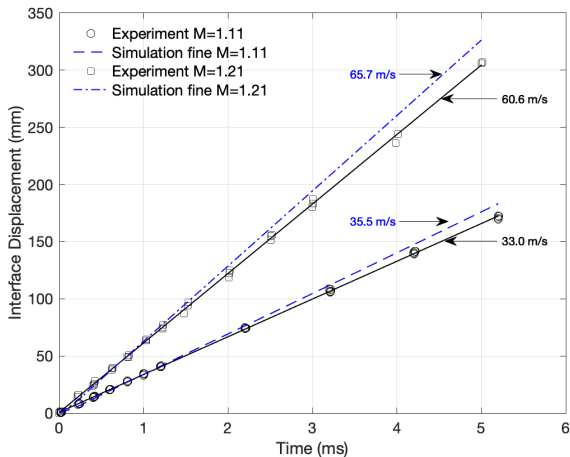


Figure – Comparison of interface displacement (mm) and interface velocity between Collins and Jacobs 2002 experiments and *FrontTier* fine grid simulations.

Problem 3 : Richtmyer-Meshkov Instability III

Comparison of amplitude between Collins and Jacobs 2002 $M = 1.11$ experiments and *Frontier* fine grid simulation.

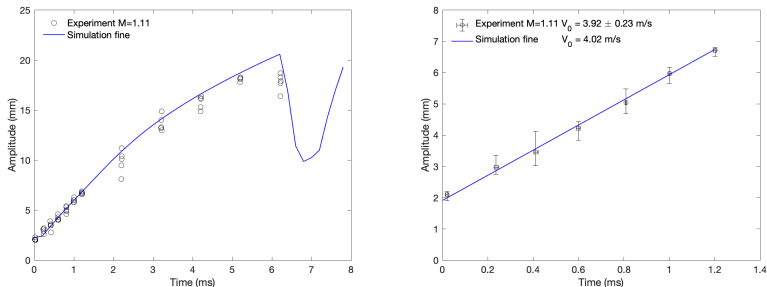
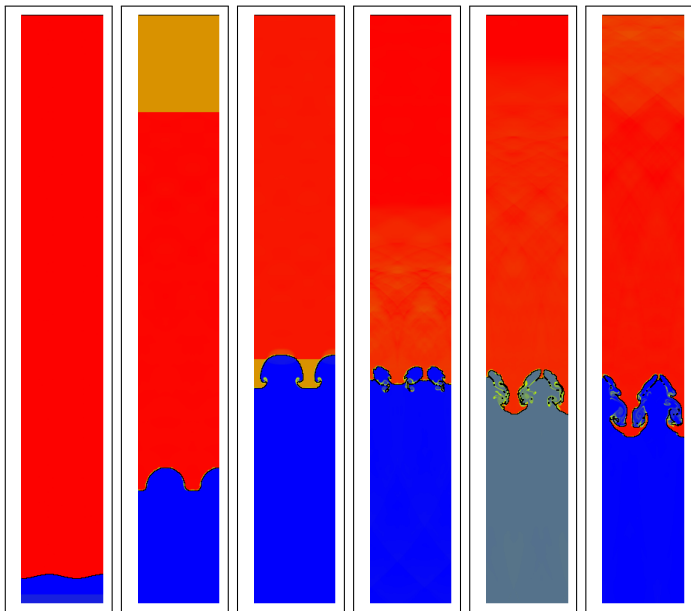


Figure – Each experimental data point with error bar in time (ms) and amplitude (mm) comes from five experiments.

	Simulation		Experiment	
	$M=1.11$	$M=1.21$	$M=1.11$	$M=1.21$
V_{intfc} (m/s)	35.5	65.7	33.0	60.6
V_0 (m/s)	4.02	5.18	3.92 ± 0.23	6.28 ± 0.6

Problem 3 : Richtmyer-Meshkov Instability IV



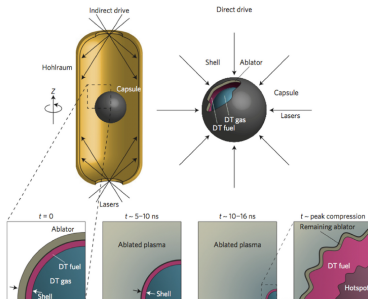
Conclusion

Single-mode shock-induced RMI simulations of an air/SF₆ interface for the Mach numbers $M = 1.11$ and $M = 1.21$ experiments of Collins and Jacobs

- Accurate and robust front tracking simulations with the fifth order WENO (Shu 2020 advises a new user to use, simple to code and generate stable and accurate result) and Yang's artificial compression reveal agreement with experimental data.
- Good agreement on the interface displacement and amplitude :
 - Mach number $M = 1.11$: Excellent agreement between the fine grid simulation and the experiment.
 - Mach number $M = 1.21$: 9% discrepancy on the early-time growth rate
- For Mach 1.21 air/SF₆ shock-tube experiments, FT simulation with 512 grid points per initial perturbed interface gives the best agreement with the experimental data.

Future Work :

- The uncertainty quantification studies to investigate the effect of model and input parameters on the growth rate and model improvement to capture the vortices at the interface are under development.
- Study the effect of higher-order WENO reconstruction on RMI.
5-9-13 perform better than 3-7-11 ?
- Explore successful ICF designs capable of achieving ignition
 - The goal is to generate a net excess of energy from this process, known as ignition, making fusion a viable alternative energy source.
 - In the design of ICF capsules, understanding the mechanisms governing the growth of RT and RM instabilities during the implosion, play an important role in achieving ignition.



Betti, R., Hurricane, O.A., 2016. Inertial-confinement fusion with lasers. *Nature Phys.* 12, 435.



47th University of Arkansas Spring Lecture Series

Numerical Linear Algebra: from Scientific Computing to Data Science Applications

May 4 - 6, 2022

Held in the Donald W. Reynolds Center for Mathematics at the University of Arkansas

A series of five lectures by
Yousef Saad
Distinguished Professor in the Department of Computer Science and Engineering at the University of Minnesota

Invited Speakers:

Mark Arnold	Agneszka Winczura
Director of Research, IBM	University of Illinois, USA
Eric Claire Carson	Khalid Moinar
State University, Ohio, USA	Ohio State, USA
Jin Chen	Sara Pulcini
IBM Research, USA	University of Illinois, USA
Alice Cvetković	Yubin Yang
PPS, London, UK	Department of Mathematics, HKU
Tim Daube	Chang Yin
Texas A&M University, USA	University of Illinois, USA

Public Lecture May 4th at 6:00 pm CST
Sabine Van Huffel
Professor Emerita in the Department of Electrical Engineering at KU Leuven

Women in STEM Panel May 6th at 1:00 pm CST

Please Register at <https://math.uark.edu>

This lecture is supported by the Donald W. Reynolds Center for Mathematics at the University of Arkansas.

For information on other programs at the University of Arkansas, please visit www.uark.edu or write to: admission@uark.edu

Headlines should be placed in the right margin of the page.

Department of Mathematical Sciences
SC200 028
11 Computer Hall, Arkansas
Fayetteville, Arkansas, 72703-1501
Telephone: (479) 575-1415
<https://math.uark.edu/>

CHALLENGES in SMART PATIENT MONITORING
from Raw Data to Decision Support

Prof. Sabine Van Huffel
KU Leuven, Dept of Electrical Engineering (ESAT)

Wednesday May 4th
6:00pm
Reynolds Centre Auditorium
2022 Department of Mathematical Sciences Public Lecture

© 2022 Department of Mathematical Sciences, University of Arkansas. All rights reserved. This document is the property of the University of Arkansas. It is not to be distributed, copied, or otherwise used without the express written permission of the Department of Mathematical Sciences. The University of Arkansas is an Equal Opportunity Institution. The University of Arkansas is an Equal Opportunity Institution. The University of Arkansas is an Equal Opportunity Institution.

UNIVERSITY OF ARKANSAS

- Dr. Jeffrey W. Jacob (University of Arizona) for providing experimental data for detailed comparison studies.
- Dr. James Glimm and Dr. Xiaolin Li (Stony Brook University)
Dr. Remi Abgrall (University of Zurich) for many helpful comments, discussions...
- Lawrence Jesser Toll Jr. Endowed Chair at the Department of Mathematical Sciences in the Fulbright College of Arts & Sciences, 2017-present.
- University of Arkansas Chancellor's Innovation Fund, 2022-2023.
- Arkansas High Performance Computing Center